Study of the electron spin resonance of negative ions field emitted into liquid helium*

Peter H. Zimmermann† and Jonathan F. Reichert
Department of Physics and Astronomy, State University of New York at Buffalo, Amherst, New York 14260

Arnold J. Dahm
Department of Physics, Case Western Reserve University, Cleveland, Ohio 44106

(Received 30 July 1976)

We report the unambiguous detection of the ESR signals of negative ions in liquid helium. The linewidth was measured to be 5.0 ± 0.4 mG, the g value was found to be pressure independent and equal to the free-electron g value to within 10 ppm, and T_1 was estimated to be greater than 100 msec. A theoretical framework has been developed which explains the microwave power and temperature dependence of the signal intensity and demonstrates the existence of an initial polarization at the time of formation of the bubble state. A striking dependence of this initial polarization on pressure was discovered. Studies have been made which apparently rule out the possibility that other species contributed to our observed signal. Extensive optical studies of a discharge region near the field emission tip have been carried out in an attempt to understand the mechanism responsible for the initial polarization. A correlation between the pressure dependences of the intensity of the ultraviolet radiation from the discharge region and the initial polarization was observed.

I. INTRODUCTION

Excess electrons injected into liquid helium have been the subject of experimental and theoretical studies for more than 15 years.[1] It is now well established that such electrons form a stable microscopically large configuration consisting of a single electron trapped inside a spherical void in the liquid of about 17-Å radius.[2] The reason for this bubble formation is quantum mechanical in nature. Due to the Pauli exclusion principle, the short-range interaction between the excess electron and the neutral helium atoms is repulsive. The weak long-range interaction of the single electron with the induced electric dipoles of the surrounding helium atoms is attractive. Thus to a first approximation, it is reasonable to consider the wave functions of the bound electron to be solutions of a noninteracting particle in a three-dimensional spherical "square" well. In its ground state, the electron is an S-state configuration. Such an isolated electron will form a two-level quantum system when placed in a uniform magnetic field. Magnetic dipole transitions between these two states should be detectable by standard electron-spin-resonance (ESR) techniques. Although these negative ions have been extensively studied, primarily by measuring their transport properties, it was only recently that some of their magnetic-resonance properties were reported.[3] ESR measurements probably would have been made long ago if it were not for the predicted long spin-lattice relaxation time and the extremely low ion densities (5×10^9 ions/cm^3) that can reasonably be obtained because of space-charge limitations.

In this paper, we shall present the results of an extensive study of this unique system. The negative ion in helium is one of the simplest bound electronic systems in nature, possibly the simplest. That is, of all bound electronic configurations in condensed matter, the electron in the helium void would be expected to have the weakest interactions with its surroundings. The measured magnetic-resonance parameters can be used to verify this theoretical expectation. This paper reports the measurements of the linewidth, g value, and signal intensity as a function of pressure and temperature. We have carried out independent experiments on the ion mobilities to verify that the charged entities we were detecting were indeed the single electron in the bubble state. Section II describes the details of the special microwave cavity, the magnetic field stabilizing and homogenizing instrumentation, and the methods used to fabricate the negative-ion field emission source. Section III reports the experimental results including the unexpected signal intensity variation with pressure, the variation of signal intensity with microwave power and ion mobility, the measurement of the g value and g value dependence on bubble diameter, the search for a positive-ion ESR signal, and the study of the signal intensity as a function of the material used for the field emission tip. Section IV details our search for charged carriers other than the electron bubble state.

The measured optical properties of the plasma discharge surrounding the field-emission tip are discussed in Sec. V. Section VI is a general discussion of the nature of the plasma and how the processes taking place in the plasma might be re-

lated to possible mechanisms for electron-spin polarization. Future experiments are considered in Sec. VII.

II. APPARATUS

A. Microwave cavity

A pressure-sealed TE_{102} mode rectangular cavity was fabricated to operate at a frequency of 13.5 GHz (*Ku* band). This cavity was designed to be compatible with the field emission sources used in this experiment. Field emission from sharp metallic tips proved to be the best method for producing the large ion densities needed in this experiment. Figure 1 shows an exploded view of the cavity. Since external high-voltage connections were needed for both the field emission tip and ion collector, special sealed and electrically insulated microwave chokes were designed to prevent microwave power from leaking out of the cavity. Such leakage reduces the cavity Q and makes the spectrometer both microphonic and unstable to any motion in its vicinity. Two cross-sectional views of these $\frac{3}{4}$-wavelength chokes are shown in Fig. 2. Locating the tip and collector in the center of the broad face of the cavity reduced the coupling of the microwave fields to these two perturbations of the simple cavity configuration. It was not possible to detect any microwave leakage outside the cavity using these chokes. Properly constructed, using carefully machined virgin Teflon dielectric, these chokes were capable of withstanding a dc potential 6.5 kV with respect to the cavity body at liquid-helium temperatures.

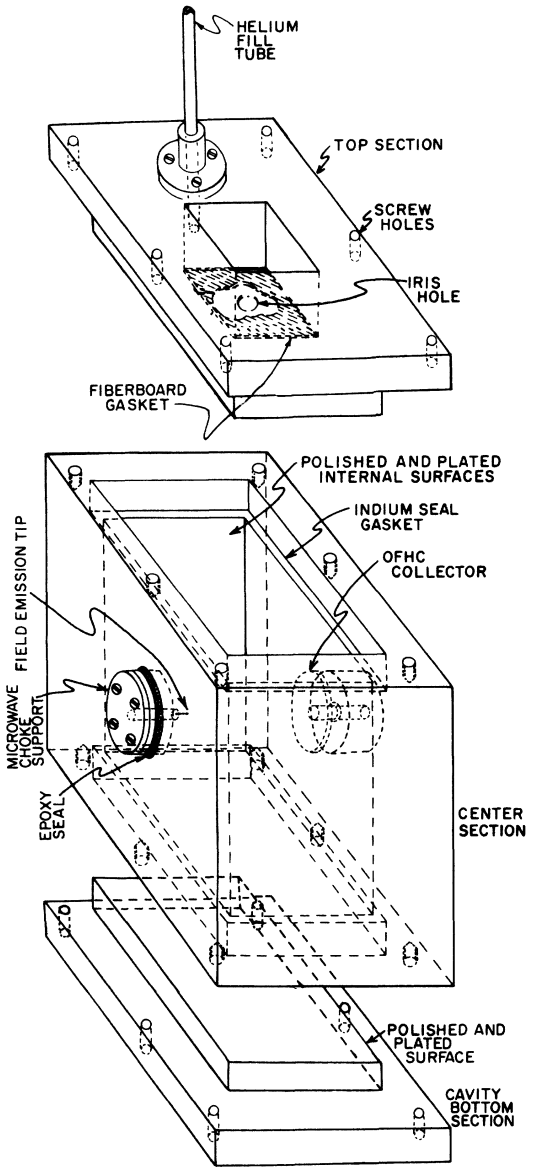

FIG. 1. Exploded view of the pressure sealed microwave cavity.

The collector caused a significant perturbation of the microwave field configuration. The presence of the collector allowed a reasonably high loaded $Q(\sim 3000)$ TE_{013} mode to be excited at a frequency near the desired frequency of the TE_{102} mode. Of course, this mode has a node of microwave magnetic field in the region that the ions traverse. Future experimenters should avoid this mode since it will dramatically reduce the observed ESR signal.

The cavity iris was pressure sealed by a simple technique. Fiberglass boards, commonly used for electronic circuit layout, proved to be a strong,

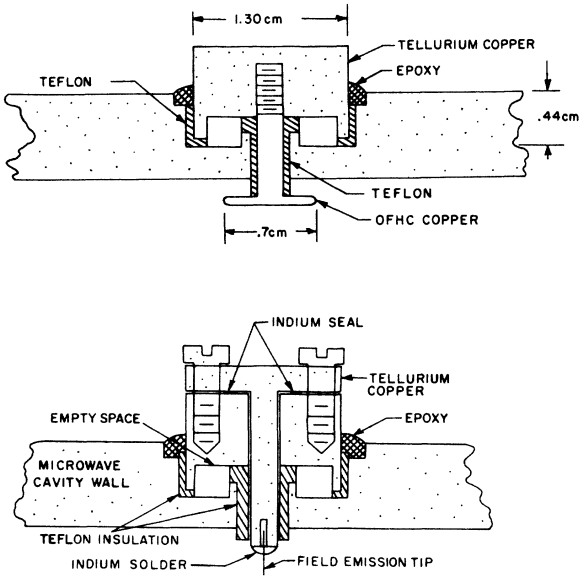

FIG. 2. Cross-sectional view of the collector and field emission tip showing the details of the electrically insulated microwave choke.

reliable, low-loss dielectric material which bonds extremely well to copper using a readily available epoxy.[4] The cavity withstood 400-lb/in.^{2} pressure at liquid-helium temperature using a 1.5-mm thick fiberboard cemented over the cavity iris. With such an arrangement, we were able to use a standard beyond cutoff dielectric variable microwave coupler for adjusting the bridge to critical coupling. The iris seal never cracked or developed leaks.

Early experiments using brass components mounted on an oxygen-free high-conductivity (OFHC) copper cavity showed the presence of strong paramagnetic materials. Such materials produce a significant temperature-dependent contribution to the dc magnetic field inside the microwave cavity and make accurate g-shift determinations difficult. In selecting appropriate materials to fabricate an optimum cavity, the following factors were considered: (i) temperature-independent diamagnetic metals, (ii) electrical conductivity, and (iii) machineability. Commercially available tellurium copper proved to be the best compromise. Although it is a much poorer electrical conductor than OFHC copper, it has about the same measured diamagnetic susceptibility and is far more machineable. To improve the cavity Q, the internal walls were electroplated with high-purity silver and gold flashed.[5] This plating proved to give no measurable additional paramagnetic fields inside the cavity. The microwave chokes, all screws, nuts, and other metallic accessories were also made of tellurium copper. The epoxy seals as well as the fiberglass board used in the microwave coupling iris were paramagnetic. Careful attempts were made to use as little of these materials as possible and still obtain reliable seals.

To facilitate fabricating the cavity, it was designed in three separate sections. This also simplified the task of plating and polishing the internal surfaces. However, such a cavity has potential microwave discontinuities at the edges where the surface current densities are large. This did not prove to be a problem. Indium seals at the joints were not only extremely reliable for sealing against superfluid helium leaks, but also were excellent conductors for microwave surface currents. Loaded cavity Q's of 10000 were readily obtained at low temperatures with these seals. The sealing surfaces were pretinned with indium to assure uniform seals of the indium joints.

It was necessary to design a cavity tuning mechanism for the measurements of g shift as a function of pressure. Because of the limited space in the Dewar and the high-voltage electrodes, the cavity tuning mechanism was placed on the bottom of the cavity. It consisted of 0.635-cm diam OFHC copper rod which was inserted into the center of the cavity. A detailed drawing of the tuning mechanism is shown in Fig. 3. This method of tuning produces a change in cavity frequency of 20 MHz per millimeter of insertion. It produces only a small degradation in Q for a total change of frequency of 60 MHz. The tuning mechanism was stable and not microphonic. The bellows seal has withstood several hundreds of cycles at low temperatures without fracturing.

B. Microwave spectrometer

Of the many types of electron-spin-resonance spectrometers that have been used for various kinds of experiments, the reflection bridge superheterodyne detector is the optimum choice for signals studied at power levels of the order of microwatts. The microwave power level required is estimated as follows. If we make the assumption that the spin-lattice relaxation time is long compared to the lifetime or transit time of the negative ion (the time it takes to traverse the microwave cavity in going from the tip to the collector), then the microwave power needed in this experiment can be estimated by considering the microwave magnetic field (H_1) necessary to cause a spin flip within a transit time. For a spin system which is described phenomenologically by the Bloch equations and which has a long T_1, the characteristic spin flip time or transition time (T) can be written as

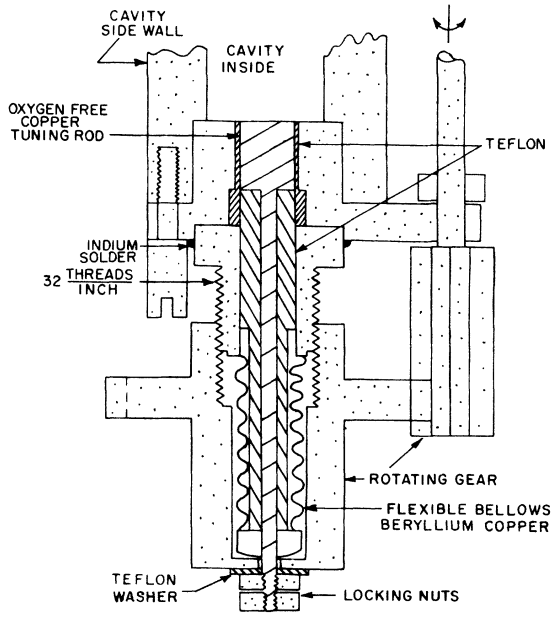

FIG. 3. Detailed cross-sectional view of cavity tuning mechanism.

$$T = \Delta H/\gamma H_1^2, \tag{1}$$

where ΔH is the linewidth of the resonance, and γ is the gyromagnetic ratio of the electron. In a typical experiment the transit time was approximately 1 msec, and the linewidth was about 20 mG. The required microwave magnetic fields are estimated [Eq. (1)] to be approximately 3 mG. The cavity Q, input power, H_1, and angular frequency ω are related by the equation

$$QP_{\text{input}} = \frac{\omega}{2\pi} \int_{\substack{\text{cavity} \\ \text{volume}}} H_1^2 \, dv. \tag{2}$$

For the cavity used in these experiments, this equation can approximately be written as

$$H_1 \approx 1.7(P_{\text{input}})^{1/2}, \tag{3}$$

where H_1 is in gauss and P_{input} is in watts. For this configuration only about 10^{-6} W of microwave power are needed to induce transitions in the spin system. At such power levels, the balanced bridge superheterodyne spectrometer is the optimum design.

Figure 4 shows a block diagram of the spectrometer. The frequency of the main klystron is phase locked to an external stabilizer and the local oscillator klystron is locked by a second phase-lock stabilizer precisely 60 MHz away from the frequency of the main klystron.[6] This stabilization scheme optimally reduces the fm noise. Imbalance did occur in the bridge because of long-term drift in the resonant frequency of the cavity. Such drift could have been eliminated by using a second slow feedback loop to adjust klystron frequency, but this would sacrifice the long-term frequency stability of the system. For typical ESR signals which have broad lines, such a slow feedback might be appropriate, but for these narrow lines and our interest in measuring absolute and relative g values, such a loop would have been counterproductive.

Another source of long-term drift (~15–20 min) in the spectrometer balance was traced to thermal expansion of the waveguide in the Dewar as the helium level dropped. A standard dc carbon resistor temperature controller was used to eliminate short-term (~30 sec) fluctuations. The long-term drifts were compensated for by fine tuning the cavity. Such tuning was accomplished by varying the temperature of the bath with corresponding changes in the dielectric constant of the liquid using the same temperature controller. The drifts were sufficiently small so that changes in bath temperature of only 0.001 K/h were needed to maintain bridge balance in the spectrometer.

Small changes in the pressure were also responsible for bridge imbalance in the spectrometer. Standard mechanical pressure regulators were not capable of sufficiently regulating the pressure of the

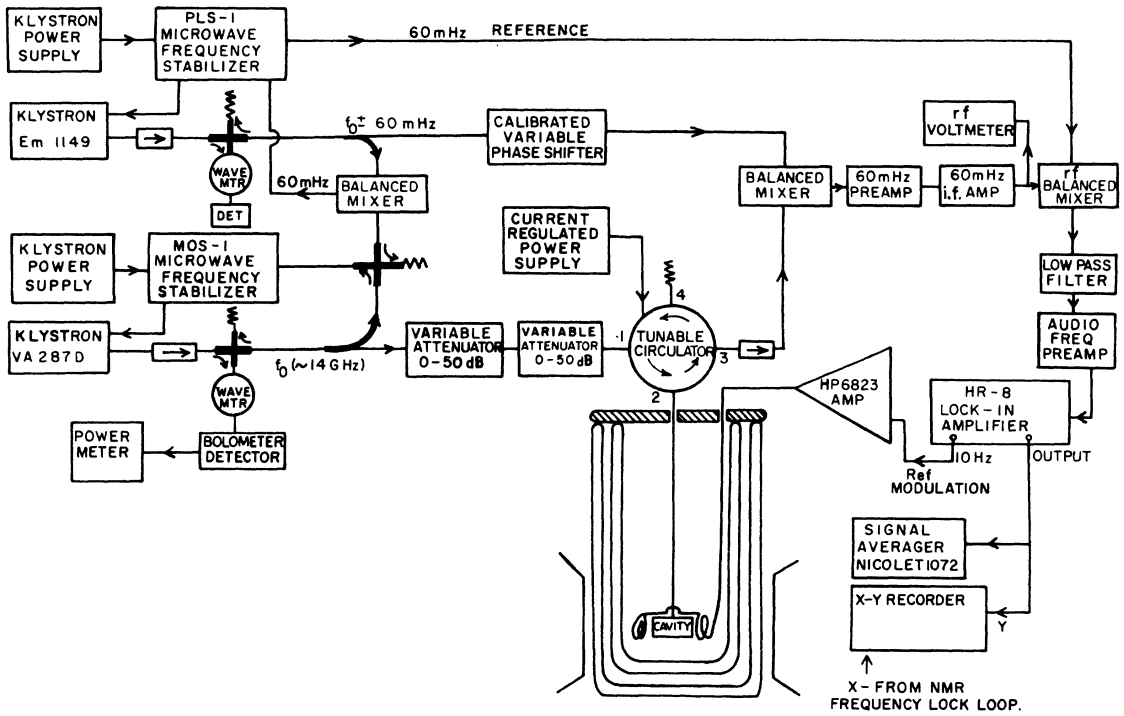

FIG. 4. Block diagram of the microwave bridge superheterodyne spectrometer.

liquid inside the microwave cavity. Pressure regulation was accomplished by connecting the cavity, through a stainless-steel fill line, to a large storage tank of helium gas at room temperature. The thermally insulated 45-l storage tank served as a ballast, which reduced the pressure fluctuations in the cavity to an unperceptably low level. Some difficulty did arise from what were believed to be Taconis oscillations in the fill tube. Various attempts were made to dampen these very-low-frequency (~0.1–1 Hz) oscillations. Small capillary fill tubes stuffed with fine multistranded nylon string were tried and although they reduced both the amplitude and the frequency oscillation, they did not eliminate them. It was empirically discovered that fill tubes of 3-mm i.d. or larger prevented these oscillations.

C. Magnetic field

The magnets designed for standard ESR experiments do not have sufficient stability and homogeneity for optimum studies of this narrow-linewidth spin system. Special modifications were made in order to improve both of these parameters for our experiments. Following Blume,[7] a special stabilizer was constructed which locked the magnetic field near the sample cavity to an external NMR frequency standard. The block diagram of this locking loop is shown in Fig. 5. The NMR probe was placed outside the Dewar (about 5 cm from the cavity center) for most experimental runs. The error signal from the phase detected cw NMR signal was fed back through a power amplifier to a small coil placed on top of the Hall sensor. The current through this coil produced a local magnetic field which was sensed by the Hall probe, and the Varian Hall circuitry responded to correct for the field in the gap. A slow servoloop was added to the system for use when the field was swept. The error signal was fed back to both the fast feedback (the coil on the Hall probe) and the slow servoloop. The servomotor mechanically swept the external sweep on the Fieldial control. The advantage in this fast-slow system is that even for sweeps of the order of 1 G, only extremely small error signal fields (~5 mG) are needed at the coil on the Hall probe. Larger magnetic fields from this coil would produce magnetic field gradients at the sample which would broaden the measured spin-resonance signal.

The magnetic field is then swept by varying the NMR frequency from the frequency synthesizer. Mineral oil was used as the proton standard in all experiments.[8] It gave strong signals with reasonably narrow lines and sufficiently short spin-lattice relaxation times. The frequency synthesizer was swept from the analog ramp voltage generated inside the signal averager. A special modification in the sweep circuit of the signal averager generated a slow sweep return ramp, which permitted recycling of the magnetic field back to its original value without the feedback circuit coming out of the lock.

This stabilization scheme was effective in drastically reducing long-term drift to less than 1 mG. Measurements of the magnetic field homogeneity, using cw NMR as well as measurements of the free induction decay of mineral oil in a pulsed NMR experiment, indicated that the field homogeneity was considerably poorer than the long-

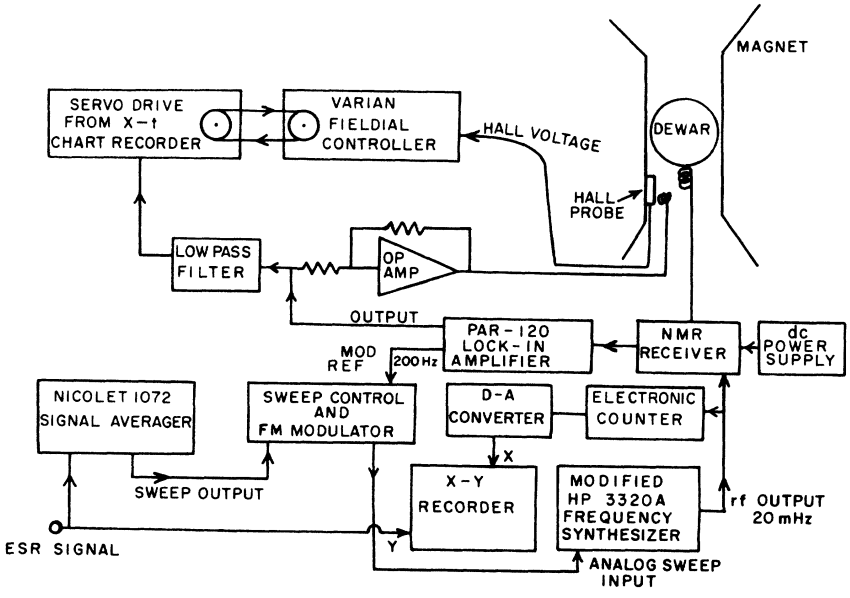

FIG. 5. Block diagram of the NMR magnetic field superstabilizer.

term stability. Specially designed electromagnetic shim coils[9] were constructed for our particular magnet gap (12-in. pole diameter, 4-in. gap). These coils produced an X, Y, Z linear gradient adjustable fields as well as one quadratic gradient correction in the direction of the main magnetic field. These coils were empirically adjusted to produce the longest free induction decay of the proton signal after a 90° pulse. Plots of the magnetic field using cw NMR also indicated a dramatic improvement in the field homogeneity across the sample volume. However, measurements of the cw NMR linewidth of protons and the ESR linewidth of the negative ion consistently gave inhomogeneities about five to ten times larger than the measured field gradients.

The reason for this discrepancy was traced to short-term instability of the magnetic field. Although the average field at the sample over a time of the order of 10 sec was uniform and stable to better than 1 mG, the short-term stability was much poorer. We attempted to improve the short-term stability by increasing the response time of the fast loop. This resulted in oscillations of the stabilizing loop. The transfer characteristics of the highly compensated Varian Hall loop produced 180° phase shifts at frequencies as low as 1 Hz. In a vain attempt to circumvent this problem, we constructed a separate fast loop to an auxiliary pair of coils on the pole pieces which had only small phase shifts in this range of frequencies. This system did not work because the Varian Hall loop sensed the magnetic field from this second loop and in attempting to cancel it caused oscillations. We were finally unable to eliminate the short-term fluctuations of the magnetic field. These field fluctuations determined the observed linewidth of the ESR signals.

Measurements of the absolute g value of the negative ion required accurate measurements of the magnetic field inside the microwave cavity during an experimental run. In order to facilitate these difficult measurements, we developed a technique for measuring the NMR resonance of room-temperature mineral oil inside a cavity immersed in liquid helium. The basic idea was to surround a small vessel of mineral oil with high-density styrofoam[10] insulation in an evacuated environment. The mineral oil was then indirectly heated by a niobium (nonmagnetic) electric heater. The heater was wrapped (noninductively) around an OFHC copper rod at one end, and the mineral oil was attached to the other end of the rod with G. E. varnish.[11] Such devices were used as magnetic field probes and were placed both inside and outside the microwave cavity for field calibration. A special bottom for the microwave cavity was used to support this NMR probe while using it to calibrate the other NMR probe permanently mounted on the outside of the cavity. The ratio of the field at the two probes was accurately established. During the actual experiment, with the inside probe removed and the tip collector installed, the magnetic field inside the cavity could be inferred from the measurements of the magnetic field at the probe outside the cavity.

D. Field emission tips

Electrons from field emission tips of tungsten, iron, and copper were used in various experiments. The 25-μm diameter metallic wire was soldered on the end of the copper support rod. Each tip was electrochemically sharpened using standard techniques.[12] Tips were examined under ×100 magnification for sharpness. It was empirically observed that tips exceeding 1.5 mm in length caused a 3-kHz oscillation in the reflected power while emitting electrons. This oscillation was attributed to mechanical vibrations of the longer tips. Shorter tips did not cause this problem. Tips that were used for many hours became blunted presumably due to positive-ion bombardment. This blunting has little effect on the magnitude of the negative-ion current.

Typical operating conditions in these experiments were tip voltage, 5.5 kV (negative with respect to ground); collector voltage, 4.5 kV (positive with respect to ground); tip current, 1.6×10^{-6} A; collector current, 1.4×10^{-6} A.

The collector and tip currents were measured with a special floating electrometer circuit employing a 741HC operational amplifier. These integrated circuit operational amplifiers could easily and cheaply be replaced in the event that a short-circuit breakdown occurred between the insulating chokes and the grounded cavity body. After about 1 h of initial breakin, where presumably tip asperities were smoothed out by ion bombardment, the tip currents stabilized and remained remarkably stable during the experimental runs. Fluctuations in this current contributed only a small fraction of the overall spectrometer noise.

III. EXPERIMENTAL RESULTS

A. Signal intensity as a function of microwave power and temperature

The paramagnetic ions that we observed differ from the standard static spin systems in that they are both created and annihilated inside the microwave cavity in a time period of the order of milliseconds. The steady-state magnetization of such a system, which might be expected to have a long spin-lattice relaxation time, can be studied by

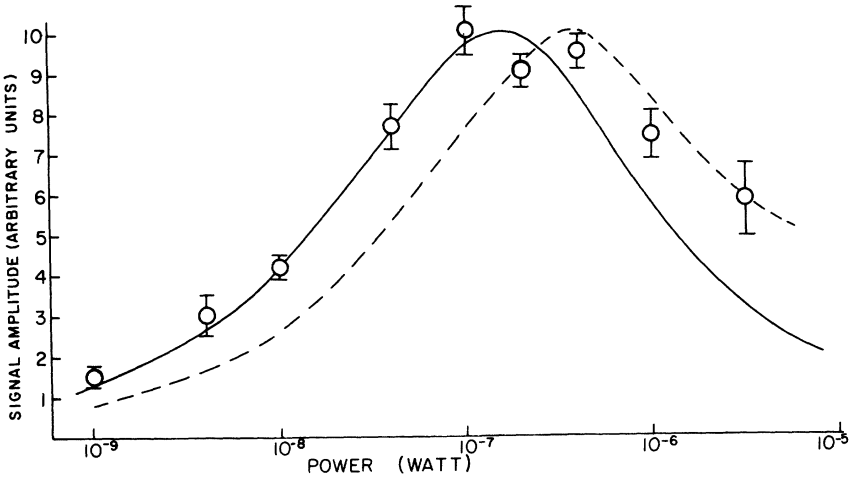

FIG. 6. Plot of the signal amplitude as a function of microwave power. The circles indicate the data for the following experimental conditions: Microwave frequency 13.420 GHz, pressure 35 Torr, temperature 1.56 K. Two theoretical curves are plotted. The dashed curve is for $\tau/T = 0.35$ at 10^{-7} W, and the solid line is for $\tau/T = 0.78$ at 10^{-7} W of microwave power.

measuring the signal intensity as function of the incident microwave power. A plot of ESR signal intensity versus microwave power is shown in Fig. 6. These data are analyzed with a theory first applied to the NMR signals of flowing liquids in the following manner.[13]

Electrons are field emitted from tungsten tips in electric fields[14] of the order of 20 MV/cm. These primary electrons, and perhaps secondary electrons created in a discharge near the tip, drift through large electric fields until they thermalize and form bubbles in regions of smaller electric fields at a distance of a few tip radii from the emitter. We shall assume that upon formation of the bubble, these negative ions have an initial magnetization M_i, and subsequently drift across the microwave cavity to the collector in a transit time τ. During this transit time, the variation of the magnetization depends upon the competition between the spin-lattice relaxation processes, which tend to drive the spin system toward its thermal equilibrium magnetization M_{eq}, and the rf induced transitions which drive the system towards saturation. The steady-state magnetization M_{ss} is related to the spin-lattice relaxation time T_1 and the linewidth as $M_{ss} = M_{eq} Z$, where

$$Z = (1 + \gamma H_1^2 T_1/\Delta H)^{-1} . \quad (4)$$

Consider the magnetization of a hypothetical pulse of ions as a function of time as it traverses the cavity. The magnetism $M(t)$ is given by

$$M(t) = M_{ss} + (M_i - M_{ss})\exp(-t/T) , \quad (5)$$

where

$$T^{-1} = T_1^{-1} + \gamma H_1^2/\Delta H . \quad (6)$$

This is illustrated in Fig. 7 for the case of $M_i > M_{ss}$, and $\tau = 0.85T$.

The time average magnetization of the pulse over the transit time is given by

$$\langle M \rangle = M_{ss} + (M_i - M_{ss})(T/\tau)[1 - \exp(-\tau/T)] . \quad (7)$$

Observe from Fig. 7 or Eq. (5) that if $M(t)$ decreases as a function of transit time, then the initial magnetization must be greater than the steady-state magnetization, which in turn can be arbitrarily small for a long T_1. It then follows from Eq. (7) that if the time average magnetization is a decreasing function of the parameter τ/T, then an initial magnetization is implied. We also note that if $M_{ss} \ll M_{eq}$, as is the case in these experiments, then by Eqs. (4) and (6) we have $T_1 \gg \Delta H/\gamma H_1^2$ and $\tau/T \simeq \gamma H_1^2/\Delta H$. Thus τ/T is proportional to the microwave power in this limit.

One may consider our sample to be a sequence of such pulses. Thus the observed magnetization is the average magnetization of these pulses. The signal intensity S from a superheterodyne bridge spectrometer is proportional to this average magnetization times the rf field H_1.[15] This can be written in the form

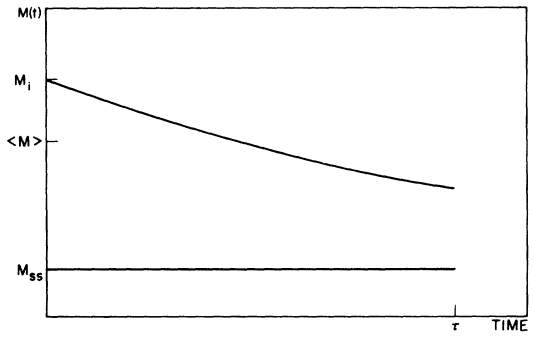

FIG. 7. An illustration of the magnetization of a pulse of electrons crossing the cavity as a function of time for $M_i > M_{ss} > 0$ and $\tau = 0.85T$.

$$S = A\langle M\rangle H_1 \ , \tag{8}$$

where $\langle M\rangle$ is given by Eq. (7), and A is a calculated parameter which depends on the cavity Q, linewidth, and spectrometer gain.

The solid and dashed lines in Fig. 6 are theoretical curves calculated from Eqs. (7) and (8) for two values of τ/T assuming $T_1 = \infty$. Using no adjustable parameters, we calculate $\tau/T = 0.9 \pm 0.4$ at 10^{-7} W of incident microwave power. The expression for calculating τ is given in Appendix A. The large error in this estimate is due to the inherent difficulties in determining the average transit time of the ions. This calculated value is in reasonable agreement with the value of 0.78×10^{-7} W which fits the data in the low-power region. It is not possible to pick a value of τ/T which fits the data over the entire range. Even if finite values of T_1 are assumed, and used to generate a family of theoretical curves, one cannot obtain a significantly better fit to the data. We offer no explanation for this discrepancy.

The mobility of the ions is strongly temperature dependent.[16] The transit time can be changed by a factor of four by varying the temperature from 1.6 to 2.1 K. However, for our space-charge limited currents,[14] which are inversely proportional to the transit time, the density of ions is independent of mobility for a fixed applied voltage. Equation (7) demonstrates that the average magnetization (for constant ion density) depends only on the ratio τ/T, and thus the temperature dependence which varies τ, and the power dependence which varies T, can be presented on a single curve. Figure 8 presents both the temperature and power dependence of the magnetization, which by Eq. (8) is proportional to the ratio $SP^{-1/2}$, on a single curve.

This universal curve clearly shows that the magnetization has the dependence on τ/T as given by Eq. (7). The decrease in magnetization with increasing values of the transit time demonstrates that an initial magnetization exists at the time the bubble state is formed.

The magnitude of the initial polarization, based on a calibration of our spectrometer with a standard sample, is approximately 1%. This may be compared with the thermal equilibrium polarization (which varies as the inverse temperature) of 20% at 1.6 K. We have assumed a temperature-independent polarization in this analysis. Adjustments based on the assumption that the initial polarization is equal to the thermal equilibrium polarization leads to a significantly poorer fit to the theoretical curve.

The steady-state magnetization represents a polarization of less than 0.2%. Since $Z = M_{ss}/M_{eq}$, the value of Z is less than 10^{-2}. Using Eq. (4), we set a lower limit on T_1 of 100 msec.

B. Signal intensity as a function of pressure

The ESR signal was observed to dramatically increase with decreasing pressure below 10 atm. at constant microwave power and temperature. Our results are shown in Fig. 9. This effect cannot be explained by the small change in mobility over this pressure range.[17] The variation in the signal is attributed to an enhanced initial polarization, possibly associated with a discharge near the

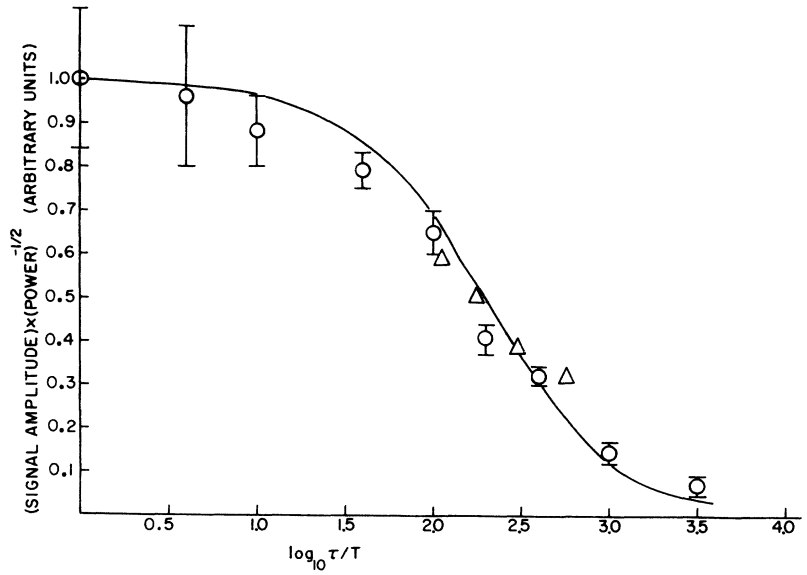

FIG. 8. Universal plot of signal amplitude divided by the square root of the power as a function of $\log_{10}\tau/T$. The solid line is a theoretical curve for $\tau/T = 0.78$ at 10^{-7} W and 1.56 K. The circles are the same data points as were used in Fig. 6. The triangles are the properly normalized data points from a constant power, variable temperature (variable τ) experiment.

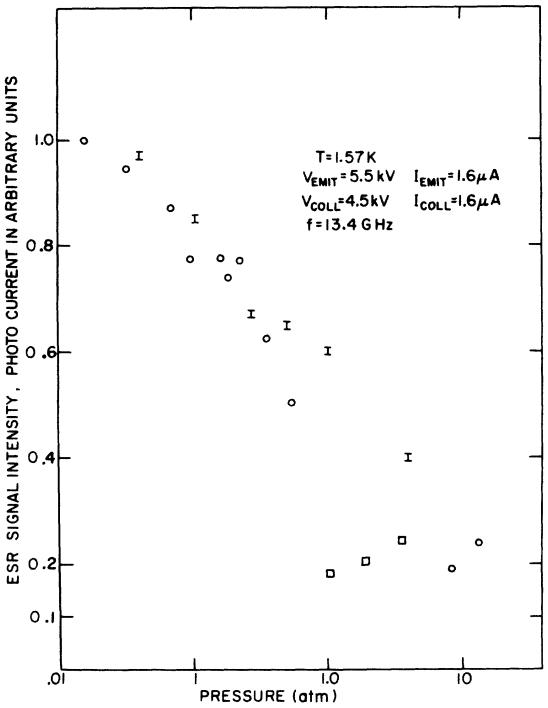

FIG. 9. ESR signal intensity as a function of liquid pressure. On the same graph is plotted the integrated intensity of ultraviolet radiation emitted from the discharge surrounding the field emission tip. The O and □ are ESR data from two independent runs. The line bars are the ultraviolet intensity data.

emitter tip. There is no evidence that any of the other ESR parameters vary with pressure.

C. Signal intensity versus emitter material

In our initial work, field emission tips were fabricated from iron whiskers with the expectation that the electrons emitted from a ferromagnetic tip would be polarized[18] and would retain this spin orientation during the process of thermalization and bubble formation. Early measurements seemed to indicate a significantly larger spin-resonance signal for electrons ejected from ferromagnetic iron tips as compared to electrons from tungsten field emitters.[3] Subsequent measurements on iron, copper, and tungsten tips showed no reproducible significant difference in the ESR signal that could be attributed to the emitter materials. The signal also did not depend on the shape of the tip. Ion bombardment caused progressive blunting of the tip during the course of a typical 10-h experimental run, but this did not affect the signal intensity.

D. *g* value

Any influence that the helium medium might have on the *g* value of the bound electron would be expected to depend on the pressure-dependent bubble radius.[19] We report both an absolute measurement of the *g* value and a measurement of its pressure dependence.

The calibration of the magnetic field inside the microwave cavity was described in Sec. IIC. The magnetic field was locked to the monitor probe just outside the cavity. The magnitude of the field inside the cavity was inferred from field ratios as measured with a second NMR probe inserted in the cavity, both before and after ESR measurements. The magnetic field was maintained near the resonant value between these two calibrations. Care was taken to sweep slowly enough to preserve the true line shape. The *g* value was determined to be equal to the free-electron *g* value to within an accuracy of one part in 10^5. The inability to reproduce the field ratio of the two NMR probes limited the accuracy with which the *g* value could be determined.

A complete absolute *g*-value measurement required the following experimental sequence: (a) a measurement of the magnetic field using an NMR probe inside the cavity; (b) removal of this probe, replacing the bottom of the cavity, and running an experiment on the ions; and (c) replacing the NMR probe and remeasuring the magnetic field. All this requires several days of running and several cycles to low temperature while maintaining constant magnetic field gradients. Thus long-term drifts in the magnetic field together with inaccuracies in repositioning the probe appeared to be the main limitations in all calibrations.

An investigation of the pressure dependence of the *g* value does not require an absolute calibration of the magnetic field. These measurements were performed in a 12-h period while keeping the magnetic field at a fixed value and locked to the NMR monitor probe and the microwave cavity maintained at a fixed temperature.

In Fig. 10, the relative *g* value is plotted as a

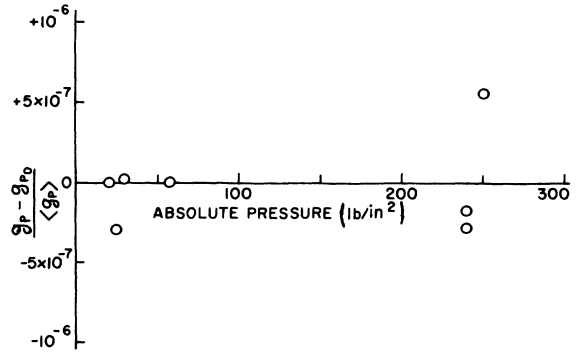

FIG. 10. Measured percentage *g* shift as a function of liquid pressure.

function of pressure. To within an accuracy of at least one part in 10^6, the g value was found to be independent of pressure over the range 21–248 lb/in.^{2} while the volume of the bubble decreased by about a factor of three. It is unlikely that any shifts at higher pressures will be observed, since the volume changes by only 30% with pressure between 250 and 400 lbs/in.^{2}

E. Linewidth measurement

The measured linewidth was consistently found to be independent of pressure, temperature, tip voltage, and tip current. We report here a linewidth (half-width at maximum derivative) of 5.0 $\pm$0.4 mG. This width is not believed to be the natural linewidth. The amplitude of the short-term fluctuations of the magnet were measured by two independent techniques and were of a magnitude which would adequately explain the measured linewidths. Larger linewidths reported earlier[3] were instrumental in origin.

F. Positive ions

A search for a positive-ion signal was also undertaken. The positive-ion current was obtained by reversing the tip and collector voltages. Since positive-ion currents were sustained at tip voltages less than those required for field ionization,[20] it is believed that positive ions are created in a discharge near the tip. Previous attempts to observe the positive-ion signals in our laboratory were unsuccessful,[3] but with the subsequent improvements in the magnetic field homogeneity and enhanced signal-to-noise ratios for the low-pressure negative-ion signals, we again attempted to observe the positive-ion signal.

The results again indicate no positive-ion signal. With the improved apparatus, a signal of at least $\frac{1}{10}$ of the negative-ion signal intensity could have been observed, an improvement by a factor of three over the previous search. Broadening of the expected signal due to close proximity of bulk molecules to the unpaired electron in the positive-ion core or a smaller initial polarization of these species may preclude the observation of an ESR signal.

IV. SEARCH FOR CHARGED CARRIERS OTHER THAN THE ELECTRON BUBBLE STATE

The experimentally measured parameters, the long spin relaxation time, the narrow linewidth, and in particular the upper limit of 10^{-5} on the deviation of the g value from the free-electron value, are characteristic of values expected for the electron isolated in a bubble in liquid helium. Nevertheless, other negatively charged entities with unknown magnetic resonance properties and with mobilities differing from the bubble state have been observed[21,22] in the temperature range $0.85 < T < 1.05$ K. These ions, called exotic carriers, were created, along with normal carriers, by Doake and Gibbon[21] in strong electric fields in the vicinity of α-particle source, and by Ihas and Sanders[22] with either a β source at the liquid surface or with a gaseous discharge in the helium vapor. Some of these same conditions, namely a strong electric field and a discharge region, exist at our electron source. One might expect that some exotic carriers would be produced. We carried out an experiment to determine whether such carriers were propagated across our chamber.

A cell similar in design to that described by Ihas and Sanders[22] was constructed to measure the mobility of charge carriers created by a field emission tip. A search for carriers with mobilities different than the normal negative-ion carrier was made throughout the pressure-temperature plane of helium II above 1.05 K. No exotic carriers were observed. An upper limit on the fraction of carriers with a specific mobility differing from the normal carrier mobility by more than 25% was set at 0.03%. The density of negatively charged entities, other than the bubble state, is insufficient to account for our signals even if a thermal equilibrium magnetization is assumed.

V. STUDY OF A DISCHARGE AT THE FIELD EMISSION TIP

Electrons field emitted into liquid helium travel through a region of large electric field (up to 20 MV/cm) before entering a smaller field and forming the bubble state as schematically shown in Fig. 11. This statement is based on theoretical calculations[23] which suggest that electrons will tunnel out of the bubble state at electric fields greater than 3 MV/cm. Our results indicate that the electrons have a net polarization when the bubble state is formed. The pressure dependence of this polarization cannot be explained if it is assumed that the polarization of the bubble state results from the field emission of polarized electrons from the metallic tip. We conclude that the electrons acquired a polarization in the time between field emission and bubble formation.

Field emission into liquid helium has been discussed in some detail in the literature.[14,24,25] We comment here on those observations which confirm that a discharge exists in the region of the tip at the vapor pressure during field emission and field ionization processes. Hysteresis in the I-V characteristics of sharp metallic tips in liquid he-

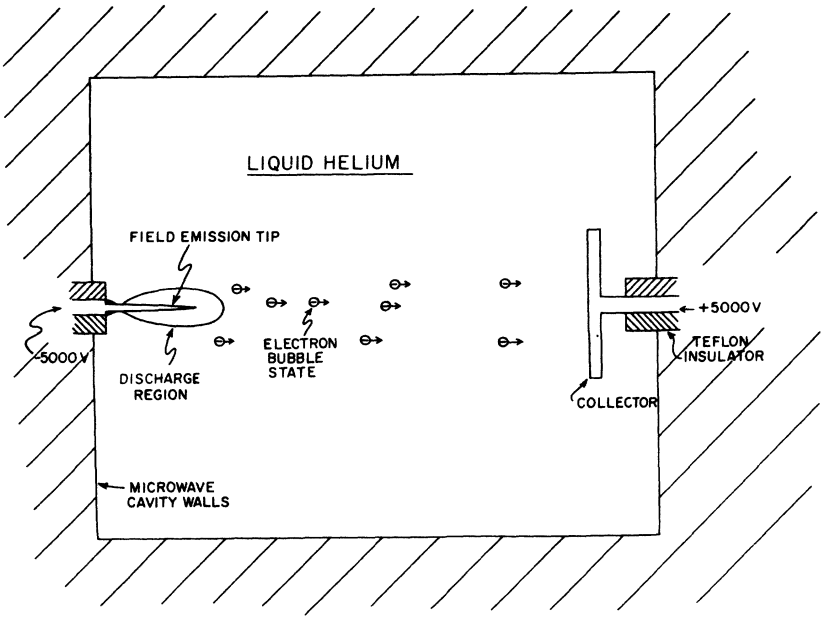

FIG. 11. Pictorial representation of the formation and motion of the negative ions in the liquid helium inside the microwave cavity.

lium have been reported for both modes.[14,20,26] This phenomenon, as well as erratic currents near threshold,[26] are characteristic of corona discharges,[27] where a higher voltage is required to initiate a discharge than to sustain it.

Hickson and McClintock[28] visually observed a discharge of radius $\simeq 10^{-2}$ cm in the region around the tip at the saturated vapor pressure for negative currents greater than 10^{-7} A. Such a large radius implies that the discharge is occurring in the vapor for the following reasons. The electric field near a tip of radius r_t decreases as $(r_t/r)^2$ from a value of 2×10^7 V/cm at the tip, and the electron is expected to form the bubble state in the liquid in fields of $\simeq 10^5$ V/cm ($r \simeq 10 r_t$). This low mobility state could not sustain the discharge, and thus if the discharge occurred in the liquid, it would have considerably smaller dimensions. The existence of a gaseous discharge at the vapor pressure is consistent with the Joule heating at the tip.

We had evidence that a discharge exists in the region near the tip not only at the vapor pressure, but at higher operating pressures as well. Hysteresis in the *I-V* characteristics and erratic currents near threshold were observed under pressures up to the melting pressure. Further evidence for a discharge was the fact that sputtering of the tip occurred during field emission under pressure, and that the tip was operated under pressure as a positive-ion source at voltages less than those required for field ionization.

An investigation of the properties of this discharge was undertaken in an attempt to understand the mechanism by which the electrons acquire a polarization as they move through this region. The spatial extent, the spectral distribution, and the intensity of the electromagnetic radiation of the discharge were measured to parameterize this region. To carry out these studies a sealed 1-cm i.d. cylindrical quartz cell was constructed and placed in an optical Dewar. A field emission tip was placed on the axis of the cell and a copper disc collector 0.95 cm in diameter was located $\simeq 0.5$ cm below the tip. Helium gas was introduced into the cell after passing through a cold trap at 77 K. These studies were carried out at 1.7 K.

A. Spatial extent of discharge

The discharge was viewed at right angles to the tip axis through a ×30 power binocular microscope with a graticule in one eyepiece. The separation of the markings on the graticule corresponded to 33 μm. The apparent shape of the discharge region was not spherical in all cases, and we defined an average discharge radius R_d such that πR_d^2 is approximately equal to the visible cross-sectional area. The value of R_d is plotted as a function of tip current for a pressure of 1 atm and as a function of pressure at a current of 1.6 μA in Figs. 12(a) and 12(b), respectively. Two sets of data are presented in each graph corresponding to data taken on a nearly virgin tip and data taken after the tip had been blunted by operating it at 2 μA for approximately 6 h. The later data were taken just before the run was terminated. The radius of the tip after the run was ≤ 1 μm and could not be determined with the use of an optical micro-

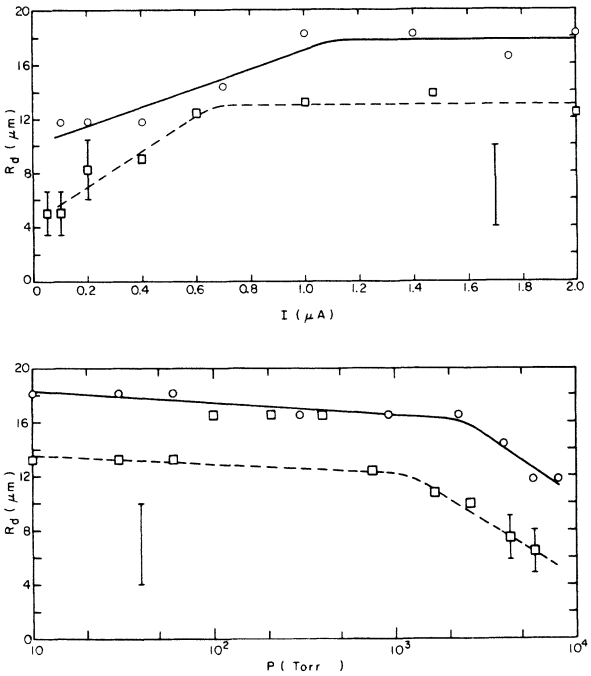

FIG. 12. Radius of the discharge at a field emitter tip operated in liquid helium at 1.7 K as measured with a × 30 power binoculars. (a) Radius vs tip current at 1-atm pressure. (b) Radius vs pressure at a tip current of 1.6 μA. The symbols represent: □ data taken with a nearly virgin tip; ○ data taken with a tip blunted with use. The lines are a guide to the eye. The uncertainties are given by the error bar unless otherwise shown.

scope. An estimate of the tip radius can be obtained with the use of the formula[29] $V/5r_t = E_t$, where V is the voltage applied to the tip, r_t is the tip radius, and E_t is the field at the tip. Near the end of the run, emission was initiated at about 4000 V which should correspond to the field $E_t \simeq 2 \times 10^7$ V/cm required for field emission into liquid helium.[14] This yields a tip radius of $\simeq 0.4$ μm.

Photographs of the discharge were taken using a different tip by imaging the discharge on the focal plane of a Polaroid camera with a lens of magnification 11 and with an exposure time of 40 sec on Polaroid-type 107 film. The tip radius was not measured, but this tip also struck at about 4000 V. This technique yielded the same variation of the discharge radius with current and pressure, but the magnitude of R_d was four times larger than the value obtained from visual observations.

B. Spectral distribution of radiation

The spectral distribution of the radiation from the discharge was studied by placing a $\frac{1}{4}$-m Jarrell-Ash scanning monochromator with a 37-Å instrumental linewidth in front of the outer window of the Dewar, approximately 4.5 cm from the tip, with no attempt made to collimate the light. Optical radiation was monitored in the range 2000–7500 Å with RCA 7326 (S-20) and EMI 6526 (S-13) photomultiplier tubes.

Thirty-six lines were observed, 18 of which were identified as atomic helium transitions and 11 as molecular helium electronic transitions.[30] No lines due to energy transfer from metastable helium states to N_2 or O_2 impurities were observed.[31]

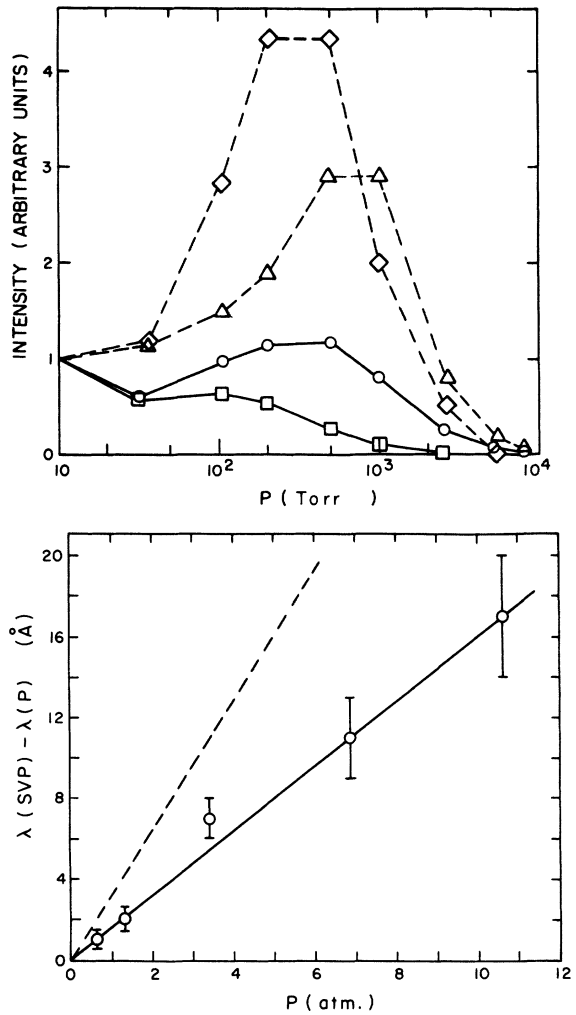

FIG. 13. (a) Relative peak intensities of four dominant lines vs pressure. The symbols represent the following transitions: □ $3\,^1S \rightarrow 2\,^1P$ (7281 Å); ○ $3\,^3S \rightarrow 2\,^3P$ (7065 Å); ◇ $D\,^1\Sigma_u^+ \rightarrow B\,^1\pi_g$ (6596 Å); and △ $d\,^3\Sigma_u^+ \rightarrow b\,\pi_g$ (6400 Å). The intensities are normalized to unity at the vapor pressure. The lines are a guide to the eye. (b) Wavelength shift of the 7065-Å line vs pressure. The solid line represents a pressure shift of −1.6 Å/atm. The dashed line represents the relative shift in wavelength with pressure (−3.2 Å/atm) for the liquid given in Ref. 33.

The singlet and triplet states were nearly equally populated. The intensity ratios of the triplet to the corresponding singlet transitions ranged from 0.3 to 3 for atomic transitions and from 3 to 6 for molecular transitions.

The pressure dependence of the peak intensity of four dominant lines, $3\,^1S-2\,^1P$ (7281 Å), $3\,^3S-2\,^3P$ (7065 Å), $D\,^1\Sigma_u^+-B\,^1\pi_g$ (6596 Å), and $d\,^3\Sigma_u^+-b\,^3\pi_g$ (6400 Å), are shown in Fig. 13(a). The relative intensities are normalized at the vapor pressure. The molecular lines shown exhibit a sharp increase in intensity at pressures on the order of 1 atm.

The wavelength shift of the 7065-Å line with pressure is presented in Fig. 13(b). The pressure shift of −1.6 Å/atm is compared with the −3.2 Å/atm shift in the liquid shown by the dashed line.[32] The absolute shift in wavelength from the vapor to the liquid reported in Ref. 32 is not shown.

C. Intensity of visible radiation

The total intensity of light emanating from the tip in the range 3100–7300 A was measured with the RCA photomultiplier tube located just outside the quartz window of the Dewar. The light intensity at a fixed temperature and pressure was proportional to the tip current in the range 10–500 nA. The ratio of the photon flux to the tip current remained constant while the tip voltage varied by factor of 7. This is a result of the fact that the voltage drop near the tip is independent of current for space-charge limited currents. (See Appendix A.) Taking into account the solid angle subtended by the photocathode, the reflection from the quartz windows, and the efficiency of the photomultiplier tube at the dominant wavelengths, we calculate one photon emitted from the discharge in the range 3100–7300 Å per 25 electrons collected.

D. Ultraviolet radiation

Ultraviolet radiation at wavelengths shorter than 1800 Å was measured by placing a photodiode consisting of a 0.95-cm diameter copper cathode and a nickel grid separated by 0.076 cm in a sealed metal chamber. The photocathode was located 1.65 cm from the tip.[33] The photodiode was tested by replacing the tip with a tritium β source and measuring both the total photocurrent due to light emitted by the electron-bombarded helium and the decrease in the photocurrent when an electric field was applied in the region of the beta tracks to prevent recombination of ion pairs. The I-V characteristics of the photodiode were analyzed with the theory of Onn and Silver[34] for electrons injected into liquid helium from a conducting surface. With an assumed quantum efficiency of 0.1 for the photocathode, we obtained a measurement of one uv photon emitted for each ion pair created by the β source and one uv photon per 5 electrons in the tip current. We estimate the latter figure to be correct to within a factor of three. As in the visible region, the ratio of photocurrent to tip current was independent of tip voltage in the range −3000 to −4000 V. Negative-ion currents were more efficient in generating uv radiation than positive-ion currents.

The most important result of our optical measurements was the correlation between the pressure dependencies of the initial polarization and the uv radiation intensity. The variation of the uv photocurrent with pressure for a fixed tip voltage and temperature is shown in Fig. 9 for tip voltages of −3000 and −4000 V. The tip current varied by less than ± 5% over the pressure range 0–4 atm.

E. Neutral excitations

Previous spectroscopic studies in the infrared and vacuum ultraviolet have shown that a large percentage of the energy of the incident electron is converted into the creation of metastable molecular states.[35] We have detected neutral excitations,[36,37] which we presume to be metastable molecular states,[38] generated by our field emission tips. At this time we are prepared to make three statements concerning these neutrals: (i) For a given tip current the signal from our neutral current detector was normally larger when the tip was operated in the field ionization mode as compared to operation in the field emission mode. (ii) Approximately one neutral excitation was created per electron in the tip current. This must be considered a crude order-of-magnitude estimate. (iii) The ratio of neutral current to tip current was independent of pressure to within our relatively large experimental errors.

VI. DISCUSSION

Our results unambiguously demonstrate that the observed ESR signal is that of the bubble state of the electron in liquid helium. The variation of the signal intensity with transit time and microwave power, the uniquely narrow linewidth, a pressure independent g value characteristic of the free electron, and the long spin-lattice relaxation time, are all experimental parameters expected for an isolated spin trapped in a void surrounded by inert-gas atoms. We have ruled out the possibility that our ESR signals are due to neutral species on the basis of the variation of signal intensity with temperature and microwave power as well as the fact that no signal was observed with positive voltages applied to the tip even though more neutral entities were detected with the tip operated in this mode.

The measured upper limit of the concentration of other charge carriers eliminates the possibility of their contribution to the observed ESR signal.

The analysis of our data shows that the electrons acquire a polarization in the region near the tip. It is reasonable to assume that this polarization occurs prior to the formation of the bubble state while the electron is interacting strongly with its environment. The mechanism which is responsible for the initial polarization is not understood at this time, but the correlation between the pressure dependencies of the initial polarization and the intensity of uv radiation strongly suggests that the polarization mechanism is related to processes occurring in the discharge.

Let us now analyze the data on the discharge presented in the previous section in an attempt to discover mechanisms which may be responsible for the polarization. There is ample evidence that the discharge occurs in the vapor state at pressures up to 10 atm. The evidence is as follows:

(a) Our measurements of the blue shift of the 7065-A atomic line with pressure is one-half of the reported wavelength shift in the liquid.

(b) The rapid growth in the occupation of the $D^1\Sigma_u^+$ and $d^3\Sigma_u^+$ states with a small increase in pressure results from an increase in the collision rate of metastable atomic states with helium atoms is not expected to occur in the liquid.

(c) No atomic or molecular transitions in the visible range at wavelengths below 6400 Å are observed in electron-bombarded liquid helium,[39,40] while we have identified 24 helium lines in the range 3000–6100 Å.

(d) All molecular transitions which have been observed in liquid helium originate on symmetric Σ states,[39,41] while we observed transitions originating on π and Δ states as well.

Visual observations of the discharge near blunted tips at large currents and low pressures yielded a discharge radius of $18 \pm 3\mu$m while photographs of the discharge gave a larger value by a factor of four. An explanation of this discrepancy may be that the intensity of the discharge does not terminate abruptly at some given R_d, and that a faint glow at larger radii was not detected visually. In our calculations we will use the value $R_d = 30$ μm.

These data show that the radius of the discharge is independent of current in the range 1–2 μA and nearly independent of pressure below 3 atm. The pressure independence is particularly surprising and may suggest that the mechanism for charge generation at low pressures is not field emission.

In order to investigate this point further we calculate the energy gained by an electron in a mean free path near the tip. The average temperature of the vapor bubble created by Joule heating near the tip at pressures greater than the vapor pressure is calculated in Appendix B under the assumption that the current is derived from field emission. The average temperature, which determines the atomic density, is approximately 50% larger than the vaporization temperature. At 1 atm of pressure we take the density of helium atoms in the vapor to be equal to the density at the normal boiling point, $n = 2.5 \times 10^{21}/\text{cm}^3$. Atomic densities of this order are supported by our wavelength-shift measurements of the 7065-Å transition. The absolute shift of this line from low-density vapor to the liquid at the vapor pressure has been measured[32] to be -5 Å. The theoretical[42] shift from the vapor to the liquid state is -19 Å with an uncertainty[43] of ± 5 Å. The data then imply that the density in the discharge at a few atmospheres is equal to the liquid density at the vapor pressure. The electron helium atom elastic collision cross section[44] is $\simeq 5 \times 10^{-16}$ cm^2, which leads to a mean free path in the vapor of $\lambda \simeq 10^{-6}$ cm. The energy gain in a mean free path near the tip is $E_t\lambda \simeq 20$ eV, and many electrons will gain enough energy to ionize helium atoms. At the vapor pressure at 1.7 K($p \simeq 10^{-2}$ atm), where the mean free path is two orders of magnitude larger, the electrons will gain sufficient energy to create a plasma of ions at large tip fields.

It seems reasonable to assume that at pressures less than a few atmospheres electrons leaving the tip initiate a cascade process in which additional electrons are formed by the ionization of helium atoms near the tip. This process can occur in electric field to density ratios too small to allow ionization of helium atoms by positive-ion bombardment, since positive ions, as opposed to free electrons, lose a large fraction of their energy in a collision. However, positive ions can bombard the tip to eject additional electrons. At larger electric fields a self-sustained discharge can occur in which helium atoms are ionized by both electron and positive-ion bombardment. At these fields the tip can be used as either a positive or negative current source. The fact that positive voltages larger in magnitude are required to use the tip as a positive-ion source[14,20] suggests that the discharge is not sustained by the ionization of helium atoms via positive-ion bombardment in the negative current mode. The field at the tip will drop below the field necessary for field emission to a pressure-dependent value sufficient to sustain the space-charge limited current. Heating near the tip will be reduced, and the approximation that the average temperature in the vapor is near the vaporization temperature is strengthened. A pressure-independent discharge radius under these conditions is more plausible than under field emission conditions.

An upper limit to the radius of the vapor bubble is also calculated in Appendix B again under the assumption that the current is derived from field emission. Our expression for the vapor bubble radius is

$$r_b \leq 10^{10} I r_t/(T_v - T_a), \tag{9}$$

where I is the tip current in amperes, T_v is the vaporization temperature, and T_a is the ambient liquid temperature. For our operating conditions at 1 atm, $I=1.6$ μA, $r_t \simeq 0.4$ μm, and $T_v - T_a \sim 2.5$ K, this expression yields a radius of 1 cm. The vapor bubble radius is certainly less than this upper limit since a large vapor region would cause a frequency shift of the microwave cavity resonance. Such a shift was not observed. The bubble radius would be much smaller if the field and hence the heating at the tip were reduced.

We are unable to determine the radius of the vapor bubble at this point, but it may be larger than the discharge radius.

A possible mechanism for the polarization of the electrons is via exchange collisions with polarized triplet metastable atoms or molecules in the discharge. To evaluate this mechanism we need a crude estimate of the production rate of triplet metastable states which can be inferred from our studies of the discharge.

Excited states of helium atoms are created in the discharge by electron bombardment. These states may then decay into metastable molecules by combining with another helium atom. We first estimate the number of singlet excited atomic and molecular states created per collected electron. The singlet states decay to the ground state via photon emission or a collision-induced nonradiative decay. The $2\,^1S_0$ state can decay by forming an $A\,^1\Sigma_u^+$ molecule which subsequently decays in the process[45,46] $A\,^1\Sigma_u^+ \rightarrow X\,^1\Sigma_g^+ + h\nu$. The $X\,^1\Sigma_g^+$ state is the unbound molecule $1\,^1S_0 + 1\,^1S_0$. This process occurs even more rapidly if the singlet metastable state escapes from the discharge into the liquid. We argue that nonradiative processes in the liquid cannot dominate the decay rate since $\simeq 30\%$ of the energy of 160-keV electrons incident on liquid helium is transformed into uv radiation.[35] The nonradiative channel is small since the potential curves for the $A\,^1\Sigma_u^+$ and $X\,^1\Sigma_g^+$ ground state do not cross at low energies.[47] This statement also applies to the vapor phase. We, therefore, assume that the uv photon production rate, 0.2 photons per electron (to within a factor of 3) is a good estimate of the generation rate of excited singlet states.

Our measured intensity ratios of the triplet to singlet lines show that triplet states are also appreciably populated in our experiment. We believe that the production rate for excited triplet states is comparable to the production rate of singlet states due to the lower threshold energy and larger impact excitation cross section for the production of the $2\,^3S_1$ atomic state.[48] From our measurements of the electromagnetic radiation and neutral excitations initiated in the discharge, we estimate 0.1–1 excited triplet states per electron in the tip current at the vapor pressure. We further assume that the metastable production rate varies as the uv intensity with pressure (see Fig. 9).

An absolute upper limit on the generation rate is obtained by dividing the voltage drop across the discharge by the lowest excitation energy of helium atoms ($\sim$20 eV). The voltage drop across the discharge is of the order of V_0, a parameter obtained from the I-V characteristic of our space-charge limited currents. A discussion of the I-V characteristic and a more precise definition of V_0 is given in Appendix A. Our experimental values of V_0 are less than 2000 V, which gives an upper limit of 10^2 metastables generated per tip electron. Since some of the energy of the electrons is converted into kinetic energy of the helium atoms, and we are only interested in the triplet component of the metastables, an absolute upper limit is $\simeq 10$ triplet metastables generated per electron. We believe this to be an overestimate based on our measurements of the uv radiation. We write the generation rate of triplets as $N_t = \gamma I/e$, where $10^{-1} \leq \gamma \leq 1$ at the vapor pressure, and $I/e = 10^{13}$ sec^{-1} for our measurements.

Our summarized conclusions drawn from the analysis of the discharge data are (i) the discharge occurs in a vapor at pressures up to and probably greater than 10 atm; (ii) at pressures less than a few atmospheres the process of electron generation is probably via positive-ion bombardment of the tip and electron multiplication by ionization of helium atoms in the discharge via electron bombardment; (iii) the discharge radius is $\simeq 30$ μm for $I > 1$ μA and $p < 3$ atm; (iv) the average temperature in the discharge is a few degrees; (v) the generation rate for triplet metastables at $I = 1.6$ μA is $\simeq 0.1$–1 per collected electron at the vapor pressure and decreases with increasing pressure as the uv intensity.

We next consider some polarization mechanisms. The insensitivity of the polarization to the tip material (tungsten, iron, or copper) and polarizations on the order of 1% from nonferromagnetic tips tend to rule out the possibility that the measured polarization results from a polarization of the electrons in the metallic tip. This independence of tip material is expected if a majority of the electrons are produced by the ionization of helium atoms in the discharge. Exchange collisions will further partially or completely destroy such a po-

larization. Ordinary spin-lattice relaxation as a polarization mechanism would appear to be ruled out because of the short lifetime as a free electron in the discharge, especially at the vapor pressure where the polarization is largest. The spin-orbit interaction is small in helium because of the small Z. In Appendix C we show that the electron leaves the discharge in $\simeq 10^{-9}$ sec. If the electron forms the bubble state at $R > R_D$, the lifetime as a free electron is $10^{-9}(R/R_D)^2$ sec.

A process consistent with our data is electron exchange in collisions with *polarized* triplet metastables. We estimate in Appendix C that the average number of exchange collisions with triplet metastable states is $N_{ex} \simeq \gamma$, where γ is the number of triplet metastable states created per collected electron ($0.1 \lesssim \gamma \lesssim 1$). If these triplet states are polarized with a polarization P_t, then this exchange process will lead to an electron polarization proportional to γP_t for $\gamma < 1$. We have argued that the uv intensity is proportional to the rate at which single metastable states are created. If we further make the ansatz that the ratio of triplet to singlet production rates are independent of pressure, then γ and hence the electron polarization will be proportional to the uv intensity. This is observed experimentally as illustrated in Fig. 9. The rapid decrease in electron polarization with increased pressure would then be explained by a decrease in the free-electron mean free path resulting in a reduced metastable production rate. We remark that the neutral current, assumed to be composed of triplet metastable molecules,[49] generated by a field emission tip was reported in Sec. V to be relatively pressure independent. However, the neutral current is a measure of the rate at which metastables escape the discharge and reach the detector, and its dependence on pressure is more difficult to predict.

There are also a number of difficulties in the above explanation. At least part of the polarization is destroyed in exchange collisions which create the triplet state. Further, we estimate in Appendix D the density of metastable states in the liquid to be a factor of ten larger than the electron density. However, we observe no signal from metastables for a g value of $\simeq 2$ with the tip operated in either the field emission or field ionization mode. This lack of signal might be explained by a linewidth which is 10^2 greater than the electron-resonance linewidth at a metastable polarization of 1%.[50] Perhaps the most disturbing feature of this mechanism is the need for a process to polarize the triplet metastable states in 10^{-5} sec. We are not aware of such a process.

Last of all scattering from polarized impurities should be considered as a polarization mechanism. Although we have taken no special precautions in purifying the helium gas introduced into our microwave cavity, we believe this process to be an unlikely candidate. Calculations analogous to those given in Appendix C show the required impurity density in the discharge to be of the order of the helium metastable density ($\simeq 10^{14}$ cm^{-3}). Such concentrations ($\gtrsim 1$ ppm) are unlikely at 2 K. Furthermore, a likely candidate for a polarized impurity would be oxygen molecules, but oxygen impurities would result in negative O_2^- ion formation. Eventually, the O_2^- atoms would be carried to the collector at the rate of 10^{13} per sec.[51] Even without this process we expect that impurities would eventually plate out on the walls of the cavity. We observe no time dependence of our signal over the period of 10 h.

Although we have been unsuccessful in determining the source of our electron polarization, we reported our results of experiments performed on the discharge in the belief that processes occurring in the discharge are related to the polarization mechanism, and with the hope that others may be able to use this data to develop a more satisfactory explanation.

VII. FUTURE EXPERIMENTS

A new magnet system is being installed which should have better than an order-of-magnitude improvement in short-term field stability. Such stability, combined with our field gradient coils, should not only dramatically increase our signal to noise, but will permit us to measure ESR linewidths of 0.5 mG. This will also permit us to measure the g shift with pressure to about 1 part in 10^7 and to set a better upper limit on the natural linewidth of the negative ion.

Experiments are underway to measure the spin-resonance properties of the negative ions in liquid ^{3}He. The magnetic nucleus of the ^{3}He atoms may have a measurable hyperfine interaction with the bound electrons, which will give us important detailed information about the electronic wave function. We are also designing a series of experiments to study the negative ion in liquid neon.

ACKNOWLEDGMENTS

We are especially indebted to W. A. Fitzsimmons for a number of communications. The authors would also like to thank T. Eck, L. Foldy, and C. C. Grimes for helpful conversations and S.C. Lau and R. Mehrotra for their technical assistance in carrying out some of the experiments.

APPENDIX A: TRANSIT TIMES

The transit time for the average carrier to move from the emitter to the collector is given by

$$\tau = \int_{r_0}^{R} \frac{dr}{\mu E(r)} . \quad \text{(A1)}$$

Here the distance r is measured from the emitter tip, μ is the mobility, $E(r)$ is the electric field, R is the emitter-to-collector separation, and r_0 is the location at which the bubble state is formed. In Eq. (A1) we have assumed a field-independent mobility and neglected the short lifetime of the electron in the free state.

A thorough treatment of the spatially dependent electric fields near field emission tips and the I-V characteristics of these tips under various conditions has been given by Halpern and Gomer.[14] Their analysis is used here. The field emission tip and collector are represented by concentric spheres of radii r_t and R, respectively. A solution of Poisson's equation in this geometry yields the following expression for the electric field,

$$E(r) = \left[\frac{8I}{3\alpha\epsilon\mu} \frac{(r^3 - r_t^3)}{r^4} + E_t^2 \left(\frac{r_t}{r}\right)^4 \right]^{1/2} . \quad \text{(A2)}$$

Here I is the total emission current, $\alpha\pi$ is the solid angle of emission, ϵ is the dielectric constant of the medium, and E_t is defined as the field at the tip which would produce the current I in the limit $\mu = \infty$ (no space-charge effects). Since I is a rapidly varying function of the tip field, E_t can be set equal to the value of the tip field at which current is first detected. In the limit of large currents, the current is given in terms of the applied voltage as

$$I = 3\alpha\epsilon\mu(V - V_0)^2/32R , \quad \text{(A3)}$$

where $V_0 = E_t r_t$. We combine Eqs. (A2) and (A3) to write

$$E(r) \simeq \left\{ \frac{(V - V_0)^2}{4Rr} + \left[E_t^2 - \frac{(V - V_0)^2}{4Rr_t} \right] \left(\frac{r_t}{r}\right)^4 \right\}^{1/2} . \quad \text{(A4)}$$

The parameter V_0 is obtained from a plot of $I^{1/2}$ versus V and varied with aging from 500 to 2000 V for tips which have been operated at low pressures at emitter-to-collector voltages equal to 6000 V.

For our typical operating conditions given in Sec. II D and with $R \simeq 1$ cm, $E_t^2 \gg (V - V_0)^2/4Rr_t$, and to within 20%

$$E(r) \simeq (V - V_0)/(4Rr)^{1/2}, \quad r > 10r_t$$

$$E(r) \simeq E_t(r_t/r)^2, \quad r < 6r_t .$$

The low mobility bubble state cannot be formed in electric fields much greater than 3 MV/cm since the electron can tunnel out of this state in larger electric fields.[23] Thus the bubble state is formed at $r_0 \gtrsim 10r_t$. Substituting the approximation for the electric field in this region into Eq. (A1), we obtain

$$\tau \simeq 4R^2/3\mu(V - V_0) . \quad \text{(A5)}$$

The transit time is insensitive to small changes in the location at which the bubble is formed since the ion spends relatively little time in the high-field region at small values of r. Since our collector is not spherically shaped, there is a spread in ion path lengths of about 10%. The value of R^2 in Eq. (A5) is an average over the square of the ion path lengths. The deviation from the assumed spherical geometry for the tip should not appreciably affect the far field for space-charge limited currents or the transit time.

In the above derivations we have implicitly assumed that the low mobility state of the ion is formed near the emitter ($r_0 \lesssim 10^2 r_t$) and that μ is independent of field for $r \gtrsim 10^2 r_t$. We consider here the effect of relaxing these assumptions. The velocity of the ion is limited to a value v_c by vortex ring creation[52] in the large fields near the tip. The correct expression for the electric field is obtained by solving Poisson's equation for the case of a constant ionic velocity[14] in the region near the tip and for a constant mobility at larger distances and requiring continuity of the electric field at a radius r_c given by $\mu E(r_c) = v_c$. The enhanced space charge in the vicinity of the tip slightly increases the far field thus partially cancelling the effect of a smaller velocity near the tip. We avoided operating conditions (large mobility and large electric field) for which this effect is appreciable when the transit time was a parameter of interest in the data analysis. Corrections due to a limiting critical velocity were less than 2%.

In the text we have shown that a discharge region of radius $\simeq 30$ μm surrounds the tip and have argued that the electrons are created in the discharge by positive-ion bombardment of the tip and by the ionization of helium atoms in the vapor rather than by field emission. For these conditions, with the low mobility state formed at a radius $r_f \gtrsim 10^2 r_t \simeq 30$ μm, our equations are altered in the following way.[14] The electric field is given by Eq. (A2) with r_t replaced by r_f, and E_t replaced by E_f, the field at the radius r_f. We rewrite Eq. (A2) with $\gamma = 8I/3\alpha\epsilon\mu$ as

$$E(r) = \left[\frac{\gamma}{r} + \left(E_f^2 - \frac{\gamma}{r_f} \right) \left(\frac{r_f}{r}\right)^4 \right]^{1/2} . \quad \text{(A6)}$$

The value of $\gamma/I = 8/3\alpha\epsilon\mu$ is approximately 40 V sec cm^{-2}. For small currents ($E_f^2 r_f \gg \gamma$) the expressions for the current and transit times are given by Eqs. (A3) and (A5) with V_0 replaced by $V_1 = V_f + E_f r_f$. Here V_f is the electric potential at r_f relative to the grounded emitter tip. The parameter V_1 is again an experimental parameter. The experimental I-V characteristics obey Eq.

(A3) which implies that $V_f + E_f r_f$ is independent of I. The parameter V_0 increases as the tip is aged.

The motion of the liquid in the cavity resulting from the force exerted on the liquid by the ions is discussed in Appendix D and decreases the transit time by 10%.

We calculated the transit time from the expression

$$\tau = (1.4 \pm 0.1) R_0^2 / \mu (V - V_0) \ , \tag{A7}$$

where R_0 is the minimum emitter-to-collector spacing, and V_0 is the zero-current intercept on a plot of $I^{1/2}$ versus V.

The uncertainties in V_0 and the positioning of the tip, which affects R_0, lead to an additional 30% error.

APPENDIX B: AVERAGE TEMPERATURE AND RADIUS OF VAPOR BUBBLE

Halpern and Gomer[14,20] calculate the temperature increase near an emitter tip and discuss the effect of the resultant vapor bubble on their I-V characteristics for both positive and negative tip currents taken at the vapor pressure. The temperature rise is a result of the localized Joule heating in the large electric fields near the tip. They assume an ideal spherical geometry with the current emitted from a sphere of radius r_t and obtain for a homogeneous medium a temperature increase given by

$$\Delta T = (I E_t r_t / 8\pi\kappa r^2)(r - r_t) \ , \tag{B1}$$

where I is the current, E_t is the field at the tip, κ is the thermal conductivity of the medium, and r is the distance from the center of the sphere. The sphere is assumed to be at the ambient temperature T_a. If a vapor bubble extends to the tip, which is probably the case for large currents, then κ is the thermal conductivity of the gas which is small and leads to a large local temperature increase. The heating is further enhanced by the fact that emission occurs from the tip through a solid angle $\Omega < 4\pi$, where $\Omega \simeq 0.6\pi$ for emitters in vacuum where space-charge effects and diffusion out of the emission cone can be neglected. If one neglects heat transfer out of the sides of the emission cone, the temperature rise within the emission cone is enhanced by the factor $4\pi/\Omega$.

Under the above assumptions, one can calculate the radius of the vapor bubble at pressures greater than the saturated vapor pressure but less than the critical-point pressure by applying the boundary condition that the temperature at the bubble radius $r_b \gg r_t$ be equal to the vaporization temperature T_v. This yields

$$r_b = I E_t r_t / 2\kappa\Omega (T_v - T_a) \ . \tag{B2}$$

This equation does not hold at the vapor pressure ($T_v = T_a$). Although the maximum temperature is large, the average temperature over the vapor bubble is

$$\langle T \rangle = T_a + \tfrac{3}{2} T_v \ . \tag{B3}$$

It is appropriate to use the thermal conductivity of helium gas at its normal boiling point, $\kappa \simeq 10^{-1}$ W/cm K, in Eqs. (B1) and (B2). Upon substitution of the values $E_t = 2 \times 10^7$ V/cm,[14] and $\Omega = 0.6\pi$ into Eq. (B2), we obtain

$$r_b = 5 \times 10^{10} I r_t / (T_v - T_a) \ , \tag{B4}$$

where I is given in amperes.

The expressions for the temperature difference and the vapor bubble radius should be considered as upper limits for the case of a field emission source since heat transfer at the side of the emission cone and the escape of photons and metastable states from the discharge have been neglected.

We have argued in the text that electron production occurs via positive-ion bombardment of the tip and the ionization of helium atoms in discharge surrounding the tip. For this case Eq. (B1) is not valid. The Joule heating is delocalized, the field in the region of the tip is reduced, and the emission cone is enlarged.[53] These effects lead to a much smaller bubble radius.

APPENDIX C: AVERAGE NUMBER OF FREE-ELECTRON EXCHANGE COLLISIONS WITH TRIPLET METASTABLES

It was estimated in Sec. VI that between 0.1 and 1 triplet metastable states were created per collected electron at the vapor pressure. We estimate here the average number of exchange collisions with these triplet metastable states that an electron undergoes in the discharge region before forming the bubble state. Such collisions outside of the discharge region will be ignored although some metastable states will diffuse out of this region, and if an electron does not form the bubble state at the edge of the discharge, additional exchange collisions may occur. In this approximation, the number of exchange collisions per electron is approximately given by

$$N_{ex} = \lambda_{ex} / l \ , \tag{C1}$$

where λ_{ex} is the mean free path for electron exchange with triplet metastable states, and l is the total distance traversed by the electron in the discharge. We assume that the electron executes a random walk to the edge of the discharge, in which case $l = R_d^2/\lambda \simeq 10^{-1}$ cm at the vapor pressure and $\simeq 10$ cm at 1 atm. The values of R_d and λ given in Sec. VI are used here. The numerical values given below will refer to the vapor pressure, and the

extrapolation to other atomic densities n in the discharge will be obvious. In traversing the distance l and electron undergoes $l/\lambda = (R_d/\lambda)^2 \simeq 10^3$ elastic collisions with helium atoms. Since electrons attain enough energy to excite helium atoms, their average energy in the discharge must be of the order of 1 eV with a velocity $v_e \simeq 10^8$ cm/sec. They exist in the discharge for a time $\tau_e \simeq 10^{-9}$ sec before entering the liquid and forming a bubble state. The electron density n_e in the vapor is $(3I/e4\pi R_d^3)$ $\tau_e \simeq 10^{11}$ cm^3.

The density of metastables in the discharge is given in steady state by equating the generation rate to the rate at which metastables either decay to ground-state helium atoms or leave the discharge. The generation rate was given in Sec. VI as $\dot{N}_t = \gamma I/e = 10^{13}\gamma$ sec^{-1}, where $10^{-1} \leq \gamma \leq 1$. The volume generation rate is $\dot{n}_t = 3\dot{N}_t/4\pi R_d^3 \simeq 10^{20}\gamma$ cm^{-3} sec^{-1}. Three mechanisms for the loss of triplet states from the discharge are considered: (1) conversion to singlet states in exchange collisions with electrons, (2) deexcitation in triplet-triplet collisions,[40] and (3) loss through the boundaries of the discharge in the liquid.

For the case where metastable decay is limited by exchange collisions with electrons each metastable is created and destroyed by an electron, and the average number of exchange collisions per electron N_{ex} is equal to γ. The lifetime of the triplet metastable is given by $\tau_t = (n_e v_e \sigma_{ex})^{-1} \simeq 10^{-5}$ sec, where $\sigma_{ex} \simeq 10^{-14}$ cm^2 is the electron metastable exchange cross section.[54] The density of triplet metastables is $n_t = \dot{n}_t \tau_t = \gamma/l\sigma_{ex} = 10^{15}\gamma$ cm^{-3}. The value of n_t varies as $\gamma/R_d^2 n$. The value $N_{ex} = \gamma$ is an upper limit.

For the metastable-metastable collision limited decay, the volume decay rate will be equal to $-\alpha n_t^2$, where $\alpha = v\sigma$ is the bilinear reaction coefficient. For thermal velocities $v \simeq 10^4$ cm sec^{-1} and a cross section[55,56] of $\sigma = 10^{-14}$ cm^2, we obtain from the equation, $\dot{n}_t = \alpha n_t^2$, a density of $\gamma^{1/2} \times 10^{15}$ cm^{-3} metastables in the discharge and a lifetime of $n_t/\dot{n}_t = \gamma^{-1/2} \times 10^{-5}$ sec for metastables. With an electron metastable exchange cross section of 10^{-14} cm^2, we obtain an electron exchange mean free path of $\lambda_{ex} = \gamma^{-1/2} \times 10^{-1}$ cm and an average of $l/\lambda_{ev} = \gamma^{1/2}$ exchange collisions per electron with metastables. The value of N_{ex} can be written explicitly as $n\sigma\sigma_{ex}\gamma^{1/2}R_d^{1/2}/(4\pi\alpha/3)^{1/2}$.

We estimate the time for metastables to diffuse through the surface of the vapor bubble as $\tau_d \simeq r_d^2/\lambda_t v \simeq 10^{-3}$ sec, where $\lambda_t = (n\sigma)^{-1} \simeq 10^{-5}$ cm is the metastable mean free path. The escape rate would be increased if the metastables had a net drift velocity through the vapor. A mechanism for a drift velocity is discussed in Appendix D, but any estimate of the drift velocity in the vapor is at best an order-of-magnitude estimate. With a superimposed drift velocity, the generation rate $10^{13}\gamma$ sec^{-1} is set equal to $\simeq n_t v_d r_d^2$. For a drift velocity v_d of 10^2 cm sec^{-1}, we obtain $n_t \simeq 10^{15}\gamma$ cm^{-3}, and a lifetime in the vapor of $\tau_t \simeq r_d/v_d \simeq 10^{-4}$ sec. The number of exchange collisions is $N_{ex} = ln_t\sigma_{ex}$ $= 10\gamma$ for values of the parameters defined above. This value is independent of R_d, but varies linearly with the density of helium atoms in the vapor. For values of $v_d < 10^3$ cm sec^{-1} the surface escape process is less efficient than electron exchange as a mechanism for the loss of metastables.

The most effective process in destroying metastables will be that process which yields the smallest value of the metastable density or since n_t $= N_{ex}/l\sigma_{ex}$, the smallest value of N_{ex}. Although some of the parameters used in our estimates are approximate, we conclude that the electron exchange process dominates, or in the worst case is competitive in the annihilation of metastables at the vapor pressure. As the pressure increases, the density of helium atoms in the vapor will increase rapidly and the value of N_{ex} for the triplet-triplet collision limited process will become very large. Thus this latter process becomes even less competitive with increased pressure. Since we have shown that the electron exchange process dominates the decay of the triplet state, we use $N_{ex} = \gamma$ for the number of collisions per electron with triplet metastables.

APPENDIX D: AVERAGE NUMBER OF METASTABLES IN THE LIQUID

In our estimate of the time average number of metastables in the liquid, we use results from our experiment on the detection of neutral excitations, assumed to be metastable molecules. A more complete discussion of the neutral excitations will appear in a later publication. We were able to show that the motion of these particles resulted from the flow of the liquid as a whole. The liquid is set in motion by the electric force on the ions which is transmitted to the fluid via collisions. Blaisse *et al.*[57] write the total force on the liquid as

$$F = \int neE\, d\tau = \int (j/\mu)\, d\tau = I\xi/\mu, \qquad \text{(D1)}$$

where n is the density of ions, E is the electric field, $d\tau$ is a volume element, j is the current density, μ is the mobility, I is the total current, and ξ is the distance traveled by the ions. The current acts as a pump in the center of the cavity setting up a flow pattern within the cavity. This flow is resisted by the frictional force at the walls of the cavity. To estimate this force we adapt the force equation for turbulent flow in a pipe.[58] The frictional force per unit area is ρv_0^2, where ρ is the

fluid density, and v_0 is a parameter characteristic of the logarithmic velocity profile near the surface defined as

$$u = (v_0/b)\ln(yv_0\rho/\eta). \quad \text{(D2)}$$

Here u is the characteristic velocity of the fluid, $b = 0.417$ cm is an experimentally determined constant, $y \simeq 1$ cm is a characteristic dimension of the cavity, and η is the viscosity. By equating the total frictional force to the force exerted by the ions, we obtain

$$A\rho v_0^2 = I\xi/\mu, \quad \text{(D3)}$$

and $v_0 \simeq 6$ cm/sec. We have used the values $A = 10$ cm^2 for the area of the cavity walls, $\rho = 0.146$ g/cm^2, $I = 1$ μA, $\xi = 1$ cm, and $\mu = 0.2$ cm^2/V sec. Upon substitution of this value of v_0 and $\eta = 10^{-5}$ poise into Eq. (D2) one obtains a characteristic velocity of $\simeq 10^2$ cm/sec. The Reynolds number is $\simeq 10^6$ consistent with the assumption of turbulent flow at the cavity walls.

We observed that to within an order of magnitude one metastable per tip electron escaped the vapor bubble and moved with the liquid. The number of metastables estimated as

$$N = I\xi/eu, \quad \text{(D4)}$$

with a transit time of $\simeq 10$ msec. Our order-of-magnitude estimate for the average number of metastables in the cavity is 10^{11} as compared with $\sim 10^{10}$ electrons.

---

*Research supported in part by the NSF under Grants No. HO39149 and No. GH40960.

†Present address: Aerospace Corp., Chemistry and Physics Laboratory, El Sequndo, Calif. 90245.

[1]For a review, see A. Fetter, *The Physics of Liquid and Solid Helium*, edited by K. H. Benneman and J. B. Ketterson (Wiley, New York, 1975).

[2]B. E. Springett, M. H. Cohen, and Joshua Jortner, Phys. Rev. 159, 183 (1967), and references therein.

[3]J. F. Reichert and A. J. Dahm, Phys. Rev. Lett. 32, 271 (1974).

[4]Alscobond Y 725 Epoxy from Emerson and Cumings, Inc., Canton, Mass. 02021.

[5]American Electroplating Corp., Cambridge, Mass. 02142.

[6]The main klystron phase-lock stabilizer was the MOS-1 and the local oscillator was stabilized using the PLS-1 both manufactured by Microwave System, E. Syracuse, N.Y., 13057.

[7]W. H. Wing, E. R. Carlson, and R. J. Blume, Rev. Sci. Instrum. 9, 1303 (1970).

[8]R. J. Allendoerfer, J. Chem. Phys. 55, 7 (1971).

[9]W. A. Anderson, Rev. Sci. Instrum. 32, 241 (1961).

[10]Styrofoam H. D. 300, Dow Chemical Co.

[11]J. F. Reichert and P. H. Zimmermann (unpublished).

[12]W. J. McG. Tegart, *The Electrolytic and Chemical Polishing of Metals* (Pergamon, New York, 1959).

[13]A. I. Zhernovoi and G. D. Latyshev, *Nuclear Magnetic Resonance in a Flowing Liquid* (Plenum, New York, 1965), p. 1.

[14]B. Halpern and R. Gomer, J. Chem. Phys. 51, 1031 (1969).

[15]G. Feher, Bell System Tech. J. 36, 449 (1957).

[16]F. Reif and L. Meyer, Phys. Rev. 119, 1164 (1960).

[17]B. Brody, Phys. Rev. B 11, 170 (1975).

[18]H. C. Siegmann, Phys. Repts. 17, 37 (1975).

[19]T. Miyakawa and D. L. Dexter, Phys. Rev. A 1, 513 (1970).

[20]B. Halpern and R. Gomer, J. Chem. Phys. 51, 1048 (1969).

[21]C. S. M. Doake and P. W. F. Gibbons, Phys. Lett. A 30, 251 (1969).

[22]G. G. Ihas and T. M. Sanders, Jr., Phys. Rev. Lett. 27, 383 (1971).

[23]S. C. Lau and A. J. Dahm, Bull. Am. Phys. Soc. 19, 460 (1974).

[24]P. V. E. McClintock, J. Low Temp. Phys. 11, 15 (1973).

[25]A. Phillips and P. V. E. McClintock, Philos. Trans. R. Soc. A278, 271 (1975).

[26]P. V. E. McClintock, Phys. Lett. A29, 453 (1969).

[27]B. L. Henson, Phys. Lett. A 33, 91 (1970).

[28]A. Hickson and P. V. E. McClintock, Phys. Lett. A 34, 424 (1971).

[29]Robert Gomer, *Field Emission and Field Ionization* (Harvard U.P., Cambridge, Mass., 1961), p. 32.

[30]A table of these transitions and their relative intensities are available from the authors.

[31]J. Jortner, L. Meyer, S. A. Rice, and E. G. Wilson, Phys. Rev. Lett. 12, 415 (1964).

[32]F. J. Soley and W. A. Fitzsimmons, Phys. Rev. Lett. 32, 988 (1974).

[33]It is well known that this type of photodiode can be used to detect metastable excitations. The placement of the photodiode was arranged to minimize detection of such neutrals.

[34]D. G. Onn and M. Silver, Phys. Rev. 183, 295 (1969).

[35]For 160-keV electrons incident on liquid helium approximately 10% of the kinetic energy of the bombarding electrons is accounted for in the production of the $A\,^1\Sigma_u^+$ molecule [M. Stockton, J. W. Keto, and W. A. Fitzsimmons, Phys. Rev. A 5, 372 (1972)] and 5% is accounted for in the production of the $a\,^3\Sigma_u^+$ molecule [J. C. Hill, O. Heybey, and G. K. Walters, Phys. Rev. Lett. 26, 1213 (1971); J. W. Keto, M. Stockton, and W. A. Fitzsimmons, Phys. Rev. Lett. 28, 792 (1972)]. Fitzsimmons later estimates the production of the $A\,^1\Sigma_u^+$ molecule to account for 30% of the incident energy [W. A. Fitzsimmons, in *Atomic Physics 3*, edited by S. J. Smith and G. K. Walters (Plenum, New York, 1973).

[36]C. M. Surko and F. Reif, Phys. Rev. Lett. 20, 582 (1968); Phys. Rev. 175, 229 (1968).

[37]R. Mehrotra, A. J. Dahm, and J. F. Reichert, Bull. Am. Phys. Soc. 21, 617 (1976). A detailed discussion of this experiment will be published elsewhere.

[38]It has been suggested by some authors that neutral excitations created in liquid helium by α particles are metastable molecular states. See W. Holcomb and J. W. Halley, J. Low Temp. Phys. 20, 365 (1975).

[39]W. S. Dennis, E. Durbin, Jr., W. A. Fitzsimmons, O. Heybey, and G. K. Walters, Phys. Rev. Lett. 23, 1083 (1969).

[40]For a review of the optical properties of liquid helium see W. A. Fitzsimmons, in *Atomic Physics 3*, edited by S. J. Smith and G. K. Walters (Plenum, New York, 1973).

[41]J. C. Hill, O. Heybey, and G. K. Walters, Phys. Rev. Lett. 26, 1213 (1971).

[42]A. P. Hickman, W. Streets, and N. F. Lane, Phys. Rev. B 12, 3705 (1975).

[43]N. F. Lane (private communication).

[44]D. E. Golden and H. W. Bandel, Phys. Rev. 138, A14 (1965).

[45]M. Stockton, J. W. Keto, and W. A. Fitzsimmons, Phys. Rev. Lett. 24, 654 (1970).

[46]C. M. Surko, R. E. Packard, G. J. Dick, and F. Reif, Phys. Rev. Lett. 24, 657 (1970).

[47]R. A. Buckingham and A. Dalgarno, Proc. R. Soc. A 213, 327 (1952).

[48]For a review and tabulated values of electron impact cross sections, see B. L. Moiseiwitsch and S. J. Smith, Rev. Mod. Phys. 40, 238 (1968).

[49]These states are expected to be triplet states since the singlet atomic state $2\,^1S_0$ in the liquid decays in 15 μsec to the $A\,^1\Sigma_u^+$ molecule by combining with another helium atom. See J. W. Keto, M. Stockton, and W. A. Fitzsimmons, Phys. Rev. Lett. 28, 792 (1972). The $A\,^1\Sigma_u^+$ molecule subsequently radiates to the ground state $1\,^1S_0 + 1\,^1S_0$.

[50]The thermal population for a magnetic field of 4800 G at 1.7 K is 18%.

[51]The plating out of oxygen impurities by electrolysis in liquid argon was reported by Harold Schnyders, Stuart A. Rice, and Lothar Meyer, Phys. Rev. 150, 127 (1966).

[52]G. W. Rayfield and F. Reif, Phys. Rev. 136, 1194 (1964).

[53]P. V. E. McClintock and H. Read-Forrest, Cryogenics 13, 371 (1973).

[54]We use an electron impact cross section characteristic of the $2\,^3S \rightarrow 2\,^1S$ and $2\,^3S \rightarrow 2\,^1P$ atomic transitions, near threshold, see B. L. Moiseiwitsch and S. J. Smith, in Ref. 48.

[55]We have taken a cross section which is approximately equal to the $2\,^3S_1 - 1\,^1D_0$ collision cross section of 1.4×10^{-14} cm^2. See E. W. Rothe, R. H. Neynaber, and S. M. Trujillo, J. Chem. Phys. 42, 3310 (1965). This latter cross section is enhanced by the attractive interaction which leads to the molecular state $a\,^3\Sigma_u^+$.

[56]Our value of $\alpha = 10^{-10}$ cm^3 sec^{-1} may be compared with values of $(2-5) \times 10^{-10}$ cm^3 sec^{-1} for the bilinear collision process $a\,^3\Sigma_u^+ + a\,^3\Sigma_u^+$ in liquid helium II reported by J. W. Keto, K. Stockton, and W. A. Fitzsimmons, Phys. Rev. Lett. 28, 792 (1972).

[57]B. S. Blaisse, J. M. Goldschvartz, and P. C. Slagter, Cryogenics 10, 163 (1970).

[58]L. D. Landau and E. M. Lifshitz, *Fluid Mechanics* (Addision Wesley, Reading, Mass., 1959), Sec. 43.